PNAS INAUGURAL ARTICLE | PHYSICS

Phase diagram of superconductivity in the integer quantum Hall regime

Jonathan Schirmer[a,1], C.-X. Liu[a,b], and J. K. Jain[a,1]

This contribution is part of the special series of Inaugural Articles by members of the National Academy of Sciences elected in 2021.
Contributed by J. K. Jain; received February 21, 2022; accepted May 11, 2022; reviewed by Nandini Trivedi and Egor Babaev

An interplay between pairing and topological orders has been predicted to give rise to superconducting states supporting exotic emergent particles, such as Majorana particles obeying non-Abelian braid statistics. We consider a system of spin polarized electrons on a Hofstadter lattice with nearest-neighbor attractive interaction and solve the mean-field Bogoliubov–de Gennes equations in a self-consistent fashion, leading to gauge-invariant observables and a rich phase diagram as a function of the chemical potential, the magnetic field, and the interaction. As the strength of the attractive interaction is increased, the system first makes a transition from a quantum Hall phase to a skyrmion lattice phase that is fully gapped in the bulk but has topological chiral edge current, characterizing a topologically nontrivial state. This is followed by a vortex phase in which the vortices carrying Majorana modes form a lattice; the spectrum contains a low-energy Majorana band arising from the coupling between neighboring vortex-core Majorana modes but does not have chiral edge currents. For some parameters, a dimer vortex lattice occurs with no Majorana band. The experimental feasibility and the observable consequences of skyrmions as well as Majorana modes are indicated.

quantum Hall effect | topological superconductivity | Majorana modes | skyrmions

Significance

Interaction between electrons leads to ordered states, such as magnets and superconductors, which have had tremendously successful technological applications. States with "topological" order have attracted much attention in recent years, canonical examples being integer and fractional quantum Hall effects, phenomena that occur when electrons in two dimensions are subjected to a magnetic field. We consider here theoretically electrons in the quantum Hall regime with superconducting correlations and find a rich phase diagram with states supporting exotic emergent entities such as "Majoranas" and "skyrmions." The former are thought to be examples of particles that are neither fermions nor bosons but obey non-Abelian statistics.

It has been nearly a century since the discovery of quantum mechanics, and yet some of its fundamental consequences are still being uncovered to this day. In particular, the role of topology in the quantum description, even for single-particle physics, had been largely ignored until the discovery of the integer quantum Hall effect (IQHE) (1), which has led to the development of topological band theory (2). In addition, a conceptually distinct but practically related development was that of quantum statistics in two-dimensional (2D) systems, which rely on the notion that two successive exchanges of a pair of particles in 2D space need not be an identity operation, as must be the case in three or higher dimensions. This fact leads to the possibility of additional types of quasiparticles, called anyons, which generalize the quantum statistics of bosons and fermions (3–5).

Superconductivity (SC), when combined with nontrivial band topology such as that found in the IQHE, can yield Majorana zero modes (MZMs), which are non-Abelian Ising anyons (6–18). (For recent experimental progress on the phenomena arising from an interplay between IQHE and SC, see refs. 19–22.) Moreover, when interacting topological states, such as the fractional quantum Hall effect (FQHE) (23), are combined with SC, even richer and more exotic classes of quasiparticles, for example parafermions and Fibonacci anyons, are thought to result. Besides being of fundamental scientific interest, anyons (particularly non-Abelian anyons) have played a role in proposals to engineer fault-tolerant topological quantum computation (10, 14, 16, 24–33).

Previous works investigating SC in quantum Hall (QH) systems have focused on proximity-coupled superconductivity, so that the SC pairing potential has been treated as an external field (20, 34–41). Because the pairing potential is not gauge invariant (it transforms with charge $2e$), the choice of the form of the (proximity-induced) pairing potential must be specified together with the gauge. A gauge invariant treatment is necessary for physical observables, such as the Chern number—a manifestly gauge-invariant quantity, since it counts edge modes of the system.

Previous works have studied the problem in the presence of a pairing field describing an Abrikosov vortex lattice—the expected ground state for type II superconductors subject to a magnetic field (39, 42, 43). These treatments do not allow for more exotic pairing order—such as half quantum vortices (HQVs), skyrmions, and giant vortices—that is possible in p-wave superconductor materials due to the multicomponent nature of the order parameter (44–52). Without a more complete, self-consistent treatment of the pairing-order parameter, one cannot establish a priori what sort of order the ground state would adopt.

Author affiliations: [a]Department of Physics, The Pennsylvania State University, University Park, PA 16802; and [b]Department of Physics, Princeton University, Princeton, NJ 08544

Author contributions: J.S., C.-X.L., and J.K.J. designed research; J.S. performed research; J.S., C.-X.L., and J.K.J. analyzed data; and J.S., C.-X.L., and J.K.J. wrote the paper.

Reviewers: E.B., Kungliga Tekniska Hogskolan; and N.T., The Ohio State University.

The authors declare no competing interest.

[1]To whom correspondence may be addressed. Email: jzs429@psu.edu or jkj2@psu.edu.

This article contains supporting information online at https://www.pnas.org/lookup/suppl/doi:10.1073/pnas.2202948119/-/DCSupplemental.

Published July 5, 2022.

Our approach in this paper is to solve the Bogoliubov–de Gennes (BdG) mean-field equations self-consistently for a model of spinless (or spin polarized) fermions with attractive interactions on a square lattice. Self-consistency guarantees gauge invariance for physically observable quantities. We do not assume a form of the pairing potential, other than its being the result of a nearest-neighbor attractive interaction, and therefore we treat the possible ground states on an equal footing. To explore all topological sectors, we find self-consistent solutions starting from many random initial guesses; we find that most of them converge to the same solution that has the lowest energy and that we identify with the ground state. We are interested in the topological nature of the ground states, which is characterized by the (superconducting) Chern number of the BdG Hamiltonian (defined below). In particular, odd SC Chern number is an indicator for the non-Abelian, or topologically nontrivial, phase of superconductivity, which is of primary interest.

A schematic of the various phases following from our calculations is shown in Fig. 1; a more detailed phase diagram is given below. We find that upon increasing the strength of the attractive interaction U, the system transitions into a superconducting phase, as expected. However, typically, the ground state does not form an Abrikosov lattice of vortices, but instead a lattice of skyrmions—where a skyrmion texture is formed by the two-component SC pairing functions and represents a domain of inverted chirality in a chiral p-wave superconductor, with half quantum vortices bound along the domain wall. In the skyrmion lattice phase, the SC Chern number is odd, and so the system hosts chiral Majorana edge modes. However, the bulk fermionic spectrum is gapped, implying that there are no MZMs in the bulk. Upon further increasing U, the system forms a square lattice of Abrikosov vortices. The MZMs located at the vortices hybridize into low-energy Majorana bands, but the ground state has an even SC Chern number, implying that the system is in a topologically trivial phase with no chiral Majorana edge modes. In addition, at some isolated points in the parameter space, a lattice of vortex dimers may compete with the vortex lattice and become the ground state. This phase, like the skyrmion phase, has chiral Majorana edge modes, because the SC Chern number is odd, but the bulk spectrum is gapped, indicating an absence of bulk MZMs.

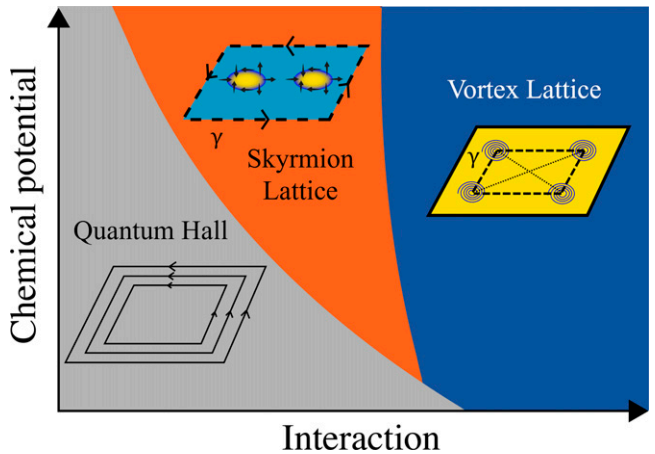

Fig. 1. A schematic phase diagram showing the phases of the model. The types of edge modes that the phases can support are indicated: The quantum Hall phase hosts chiral fermionic edge modes (solid lines); the skyrmion lattice phase hosts chiral Majorana edge modes (dashed lines labeled with γ); the vortex lattice phase hosts either fermionic edge modes or no edge modes at all. In the vortex lattice phase, the Majorana excitations, which in a chiral p-wave supeprconductor are bound to vortices, hybridize between proximate vortices (depicted via dashed lines between vortices) and open a low-energy spectral gap. In the skyrmion lattice phase the yellow and blue colors indicate different chiralities of the superconducting order parameter, and the arrows depict the direction of a pseudospin vector (defined in the main text).

Model

We start with the interacting Hamiltonian, which is defined on a square lattice with unit lattice constant as

$$\begin{aligned}\mathcal{H} &= \mathcal{H}_0 + \mathcal{H}_I \\ \mathcal{H}_0 &= -\sum_{j,\delta}\left(e^{iA_{j+\delta,j}}\hat{c}^\dagger_{j+\delta}\hat{c}_j + e^{iA_{j,j+\delta}}\hat{c}^\dagger_j\hat{c}_{j+\delta}\right) - \mu\sum_j \hat{c}^\dagger_j\hat{c}_j \\ \mathcal{H}_I &= -U\sum_{j,\delta}\hat{c}^\dagger_{j+\delta}\hat{c}^\dagger_j\hat{c}_j\hat{c}_{j+\delta}, \end{aligned} \quad [1]$$

where $\hat{c}^\dagger_j$ ($\hat{c}_j$) creates (annihilates) a spinless fermion on site j, located at position $\boldsymbol{r}_j$, and $\hat{c}^\dagger_{j+\delta}$ ($\hat{c}_{j+\delta}$) creates (annihilates) a spinless fermion on a site that is a nearest neighbor to site j, located at position $\boldsymbol{r}_j + \hat{\delta}$, where $\delta = x, y$. The chemical potential is μ, the interaction strength is $-U$ with $U > 0$, and the external magnetic field is incorporated through complex hopping matrix elements with phases $A_{j+\delta,j} = -A_{j,j+\delta}$. We measure all energies in units of the hopping amplitude. The set of hopping phases encodes the magnetic flux Φ_j through each square lattice plaquette

$$2\pi\frac{\Phi_j}{\Phi_0} = A_{j+\hat{x},j} + A_{j+\hat{x}+\hat{y},j+\hat{x}} - A_{j+\hat{x}+\hat{y},j+\hat{y}} - A_{j+\hat{y},j}, \quad [2]$$

where $\Phi_0 = h/e$ is the flux quantum.

In the presence of an external magnetic field, the noninteracting part of the Hamiltonian $\mathcal{H}_0$ does not commute with translations by a single site. Therefore, the unit cell must be enlarged into the so-called magnetic unit cell (MUC) that encloses an integer number of flux quanta (53). The noninteracting part of the Hamiltonian $\mathcal{H}_0$ commutes with translations defined by the operators $T_{\boldsymbol{R}} = \sum_j \hat{c}^\dagger_{j+\boldsymbol{R}}\hat{c}_j$, where $\boldsymbol{R}$ is a translation vector corresponding to the MUC. It is possible to choose a vector potential such that e^{iA} has spatial period $\boldsymbol{R}$ (see next paragraph), thus ensuring that

$$[\mathcal{H}_0, T_{\boldsymbol{R}}] = \sum_{j,\delta}\hat{c}^\dagger_{j+\boldsymbol{R}+\delta}\hat{c}_j\left(e^{iA_{j+\delta,j}} - e^{A_{j+\boldsymbol{R}+\delta,j+\boldsymbol{R}}}\right) \quad [3]$$

vanishes. We choose the MUC lattice vectors $\boldsymbol{R}_1 = M\hat{\boldsymbol{y}}$ and $\boldsymbol{R}_2 = N\hat{\boldsymbol{x}}$, with precisely h/e flux through the MUC.

The phases $A_{j+\delta,j}$ are periodic only if the total magnetic flux through the MUC is zero. This can be ensured by performing a singular gauge transformation that inserts a point flux of $-h/e$ through a single square plaquette in the MUC to cancel the total flux. We emphasize that the insertion of the point flux, having magnitude h/e, has no effect on any physical observable and is therefore a pure gauge transformation. To fix the gauge we impose the condition $A_{j+\hat{x}+\hat{y},j+\hat{x}} = A_{j+\hat{x}}$ for all sites j, and the point flux is chosen to pass through the lower right plaquette of the MUC; with these conditions, the set of linear equations (Eq. **2**) uniquely fixes the gauge. See *SI Appendix* for an example of our gauge-fixing scheme.

To proceed with mean-field theory in real space, we consider an alternative Hamiltonian $\mathcal{H}_{\mathrm{MF}}$ obtained by replacing the interaction term in $\mathcal{H}$ by fermion bilinears coupled to fields. The

Hamiltonian, after the standard mean-field decomposition in the pairing channel, is

$$\mathcal{H}_{\rm MF} = -\sum_{j,\delta}\left(e^{iA_{j+\delta,j}}\hat{c}^\dagger_{j+\delta}\hat{c}_j + e^{iA_{j,j+\delta}}\hat{c}^\dagger_j\hat{c}_{j+\delta}\right) - \mu\sum_j \hat{c}^\dagger_j\hat{c}_j - \sum_{j,\delta}\left(\Delta_{j,\delta}\hat{c}^\dagger_{j+\delta}\hat{c}^\dagger_j + \Delta^*_{j,\delta}\hat{c}_j\hat{c}_{j+\delta} - \frac{|\Delta_{j,\delta}|^2}{U}\right), \quad [4]$$

where the vector field $\Delta_{j,\delta}$ is treated as a variational parameter whose optimal value is given by

$$\Delta_{j,\delta} = U\langle\hat{c}_j\hat{c}_{j+\delta}\rangle, \quad [5]$$

where the expectation value is with respect to the ground state of the mean-field Hamiltonian $\mathcal{H}_{\rm MF}$. The Hamiltonian is invariant under the gauge transformation $\hat{c}_j \to e^{i\phi_j}\hat{c}_j$, $\Delta_{j,\delta} \to e^{i(\phi_{j+\delta}+\phi_j)}\Delta_{j,\delta}$, and $A_{j+\delta,j} \to A_{j+\delta,j} + \phi_{j+\delta} - \phi_j$.

We consider a lattice with $L \times L$ MUCs, with each MUC of size $M \times M$; we take $L = 10$ and $M = 20$ for our numerical calculations. We write the mean-field Hamiltonian in momentum space by Fourier transforming $\hat{c}_j = \frac{1}{L}\sum_{\boldsymbol{k}} e^{i\boldsymbol{k}\cdot\boldsymbol{R}}\hat{c}_\alpha(\boldsymbol{k})$, where $\boldsymbol{R}$ is the position vector for the origin of the MUC in which site j lies and α is a site label within the MUC corresponding to site j. The number of allowed $\boldsymbol{k}$ magnetic momenta is L^2. We have tested that our results do not change qualitatively when larger values of L are used.

Assuming that the pairing field $\Delta_{j,\delta}$ has the same periodicity as the MUC, we obtain the mean-field Hamiltonian in the BdG form

$$\mathcal{H}_{\rm MF} = \frac{1}{2}\hat{C}^\dagger(\boldsymbol{k})\mathcal{H}_{\rm BdG}(\boldsymbol{k})\hat{C}(\boldsymbol{k}) + \frac{1}{2}\sum_m\left(\epsilon_m(\boldsymbol{k}) - \mu\right) + \sum_{j,\delta}\frac{|\Delta_{j,\delta}|^2}{U}, \quad [6]$$

where $\epsilon_m(\boldsymbol{k})$ are the eigenenergies of the noninteracting Hamiltonian $\mathcal{H}_0$. The row vector $\hat{C}^\dagger(\boldsymbol{k}) = \left(\hat{c}^\dagger_1(\boldsymbol{k})\ \cdots\ \hat{c}^\dagger_{M^2}(\boldsymbol{k})\ \hat{c}_1(-\boldsymbol{k})\ \cdots\ \hat{c}_{M^2}(-\boldsymbol{k})\right)$ and

$$\mathcal{H}_{\rm BdG}(\boldsymbol{k}) = \begin{pmatrix} h(\boldsymbol{k}) & \Delta_{\rm A}(\boldsymbol{k}) \\ \Delta^\dagger_{\rm A}(\boldsymbol{k}) & -h^*(-\boldsymbol{k})\end{pmatrix}, \quad [7]$$

where $\Delta_{\rm A}(\boldsymbol{k}) = \Delta(\boldsymbol{k}) - \Delta^T(-\boldsymbol{k})$ and $\Delta(\boldsymbol{k})$ is the Fourier transform of $\Delta_{j,\delta}$. The BdG Hamiltonian $\mathcal{H}_{\rm BdG}(\boldsymbol{k})$ is $2M^2 \times 2M^2$, Hermitian, and so is diagonalizable by a unitary transformation. We write the quasiparticle operators, which are the eigenoperators of the Hamiltonian $\mathcal{H}$, as

$$\hat{\gamma}_m(\boldsymbol{k}) = \sum_\alpha u_{\alpha,m}(\boldsymbol{k})\hat{c}_\alpha(\boldsymbol{k}) + v_{\alpha,m}(\boldsymbol{k})\hat{c}^\dagger_\alpha(-\boldsymbol{k}), \quad [8]$$

where $u_{\alpha,m}(\boldsymbol{k})$ and $v_{\alpha,m}(\boldsymbol{k})$ are determined from the eigenvectors of $\mathcal{H}_{\rm BdG}(\boldsymbol{k})$, and m labels the BdG quasiparticle bands. Note that the BdG Hamiltonian is particle–hole symmetric

$$\mathcal{P}\mathcal{H}_{\rm BdG}(\boldsymbol{k})\mathcal{P}^{-1} = -\mathcal{H}_{\rm BdG}(-\boldsymbol{k}), \quad [9]$$

where $\mathcal{P} = \tau_x\mathcal{K}$, $\mathcal{K}$ is the complex conjugation operator, and τ_x is a Pauli matrix acting on the particle and hole subspaces. This means that not all eigenvectors are independent—if $\begin{pmatrix}\boldsymbol{V}_1(\boldsymbol{k}) & \boldsymbol{V}_2(\boldsymbol{k})\end{pmatrix}^T$ is an eigenvector of $\mathcal{H}_{\rm BdG}$ at positive $E(\boldsymbol{k})$, then $\begin{pmatrix}\boldsymbol{V}_2(\boldsymbol{k})^* & \boldsymbol{V}_1(\boldsymbol{k})^*\end{pmatrix}^T$ is an eigenvector of $\mathcal{H}_{\rm BdG}$ at $-E(-\boldsymbol{k})$. This, in turn, implies that not all quasiparticle operators are independent

$$\hat{\gamma}_m(\boldsymbol{k}) = \hat{\gamma}^\dagger_{m'}(-\boldsymbol{k}), \quad [10]$$

where band m' is such that $E_m(\boldsymbol{k}) = -E_{m'}(-\boldsymbol{k})$. Given all this, the full Hamiltonian $\hat{H}$ can be expressed as

$$\mathcal{H}_{\rm MF} = \sum_{\boldsymbol{k}}\sum_{m=1}^{M^2}\left(E_m(\boldsymbol{k})\hat{\gamma}^\dagger_m(\boldsymbol{k})\hat{\gamma}_m(\boldsymbol{k}) + \frac{1}{2}\epsilon_m(\boldsymbol{k}) - \frac{1}{2}E_m(\boldsymbol{k})\right) + \sum_{j,\delta}\frac{|\Delta_{j,\delta}|^2}{U}. \quad [11]$$

The ground-state energy is given by

$$E_g = \sum_{E_m(\boldsymbol{k})<0}E_m(\boldsymbol{k}) + \frac{1}{2}\sum_{\boldsymbol{k}}\sum_{m=1}^{M^2}\left(\epsilon_m(\boldsymbol{k}) - \mu - E_m(\boldsymbol{k})\right) + \sum_{j,\delta}\frac{|\Delta_{j,\delta}|^2}{U}. \quad [12]$$

By inverting Eq. **8**, we can express the expectation value $\langle\hat{c}_j\hat{c}_{j+\delta}\rangle$ in terms of $u_{\alpha,m}(\boldsymbol{k})$ and $v_{\alpha,m}(\boldsymbol{k})$ (at zero temperature) to write the self-consistency equation Eq. **5** as

$$\Delta_{j,\delta} = \frac{U}{L^2}\sum_{\boldsymbol{k}}\sum_m e^{-i\boldsymbol{k}\cdot\Delta\boldsymbol{R}}u_{\alpha+\delta,m}(\boldsymbol{k})v^*_{\alpha,m}(\boldsymbol{k}), \quad [13]$$

where α is the site within the MUC corresponding to site j and $\Delta\boldsymbol{R}$ is difference in MUC location of site $j+\delta$ and site j. The subscript $\alpha+\delta$ refers to the nearest neighbors of site α and is understood to be taken modulo the MUC. This equation is solved iteratively by starting with a random guess for the pairing potential $\Delta^{(0)}_{j,\delta}$, diagonalizing $\mathcal{H}_{\rm BdG}$ to obtain u_αs and v_αs, and then obtaining a new pairing potential $\Delta^{(1)}_{j,\delta}$ using Eq. **5**. The new pairing potential is treated as a new guess and the process is repeated until convergence is achieved to within a relative error of 10^{-5}. Many random initial guesses are tried, and the one that yields the lowest energy (expressed in Eq. **12**) is taken to be the ground-state solution. Generically, a large majority of the initial guesses produce the ground state. Solutions with higher energies than the ground state are taken to be excited states. We emphasize that the solutions to the self-consistency equation are gauge invariant in the sense that if $\Delta_{j,\delta}$ is a solution to the self-consistency equations with energy E_g in a certain gauge, then $e^{i(\phi_{j+\delta}+\phi_j)}\Delta_{j,\delta}$ is a self-consistent solution in another gauge, related to the first one by the gauge transformation ϕ_j, with the same energy E_g.

The BdG Hamiltonian $\mathcal{H}_{\rm BdG}(\boldsymbol{k})$, describing a system in two spatial dimensions and being particle–hole symmetric only, resides in class D of the Altland–Zirnbauer classification (54) and is therefore characterized by a $\mathbb{Z}$ bulk topological invariant, called the Chern number $\mathcal{C}$ (2). For superconducting systems, the Chern number $\mathcal{C}$ counts the number of chiral Majorana edge modes (6, 12, 13, 15) and, in particular when $\mathcal{C}$ is odd, the system is topologically distinct from an ordinary quantum Hall state that, in the BdG framework, possesses an even Chern number. The Chern number of the BdG Hamiltonian can be computed in the same fashion as for noninteracting Hamiltonians: One defines the Berry connection, determined by the eigenvectors $|u^m(\boldsymbol{k})\rangle$ of the BdG Hamiltonian $\mathcal{H}_{\rm BdG}(\boldsymbol{k})$, where m labels the band, as

$$A^{mn}_\mu(\boldsymbol{k}) = i\langle u^m(\boldsymbol{k})|\partial_\mu|u^n(\boldsymbol{k})\rangle, \quad [14]$$

where ∂_μ is the shorthand for $\partial/\partial k_\mu$. The Berry curvature is then defined as

$$F^{mn}_{\mu\nu}(\boldsymbol{k}) = \partial_\mu A^{mn}_\nu - \partial_\nu A^{mn}_\mu + i\,[A_\mu, A_\nu]^{mn}. \quad [15]$$

The only nonzero components of the Berry curvature are $F_{xy} = -F_{yx} \equiv F$. The Chern number is then given by the Berry curvature integrated over the magnetic Brillouin zone (MBZ):

$$\mathcal{C} = \frac{1}{2\pi}\int_{\mathrm{MBZ}} d^2k\,\mathrm{Tr}\,[F(\boldsymbol{k})]_{E(\boldsymbol{k})<0} \quad [16]$$

We compute Eq. **16** numerically using the method of Fukui et al. (55)—the Berry curvature is determined on a grid in a discretized MBZ by defining

$$M^{mn}_\lambda(\boldsymbol{k_\alpha}) = \langle u^m(\boldsymbol{k_\alpha})|u^n(\boldsymbol{k_\alpha}+\boldsymbol{e}_\lambda)\rangle. \quad [17]$$

The points on the grid are labeled by $\boldsymbol{k_\alpha}$ and the spacing vectors are $\boldsymbol{e}_\lambda$, where $\lambda = 1, 2$. In terms of the link variables defined as

$$U_\lambda(\boldsymbol{k_\alpha}) = \frac{\det M_\lambda(\boldsymbol{k_\alpha})}{|\det M_\lambda(\boldsymbol{k_\alpha})|} \quad [18]$$

the discrete Berry curvature at each point on the grid is given by

$$\tilde{F}(\boldsymbol{k_\alpha}) = \ln\Big(U_1(\boldsymbol{k_\alpha})\,U_2(\boldsymbol{k_\alpha}+\boldsymbol{e_1})\,U_1^{-1}(\boldsymbol{k_\alpha}+\boldsymbol{e_2})\,U_2^{-1}(\boldsymbol{k_\alpha})\Big). \quad [19]$$

The Chern number is then given by

$$\mathcal{C} = \frac{1}{2\pi i}\sum_{\boldsymbol{\alpha}} \tilde{F}(\boldsymbol{k_\alpha}). \quad [20]$$

Results

We are primarily interested in the ground state and the low-energy fermionic spectrum of the model. Indeed, we find a rich phase diagram with unexpected ground states, as shown in Fig. 2, which we discuss in detail below.

A. Quantum Hall Phase. Superconducting regions in the phase diagram are denoted with color (Fig. 2*A*), and the nonsuperconducting region is indicated in white, where the single-particle spectrum forms very flat and nearly equally spaced Landau level-like Chern bands (we henceforth refer to them as LLs), with superconducting Chern number $\mathcal{C} = -2\nu$, where ν is the filling factor (56). The energy of these bands is indicated by the horizontal black lines in Fig. 2*A*, and this phase is deemed a QH phase.

It should be noted that if the chemical potential is tuned to lie precisely within a LL, superconductivity extends to arbitrarily low interaction strength. The indicated boundary between the QH and the superconducting regions (dashed line in Fig. 2) is determined for chemical potentials that lie halfway between LLs.

B. Skyrmion Phase. Starting from the nonsuperconducting region and increasing the attractive interaction strength, the QH system transitions into a superconducting ground state that forms a skyrmion lattice (44, 46, 48, 49, 51, 52) (discussed below at more length) for values of the chemical potential corresponding to filling factor $\nu \gtrsim 3$. This region is indicated in red in Fig. 2. The SC Chern number $\mathcal{C}$ changes rapidly near the phase boundary (narrow regions with high $\mathcal{C}$ have not been indicated in the phase diagram for simplicity), attaining the value $\mathcal{C} = -1$ slightly away from the phase boundary. The phase boundary also has an oscillatory dependence on the chemical potential, not shown in Fig. 2.

In a chiral p-wave superconductor, a skyrmion is a closed domain of inverted chirality with half-quantum vortices (HQVs) located on the domain wall (44, 46, 48, 49, 51, 52). As shown below, these configurations have a skyrmionic texture in a suitable pseudospin representation and carry a nonzero topological charge. The magnitudes of the two components of the order parameter, $|\Delta_{j,x}|$ and $|\Delta_{j,y}|$; the particle density; and the low-energy BdG quasiparticle band structure are shown in Fig. 3 *A*–*D*. It can be seen that there are two vortices per component of the order parameter that each have different locations (the vortices are coreless). The phase of only one component of the order parameter winds by 2π around each vortex while the other component remains constant. The vortices are HQVs since each one is associated with a $h/4e$ magnetic flux (the entire skymion in each

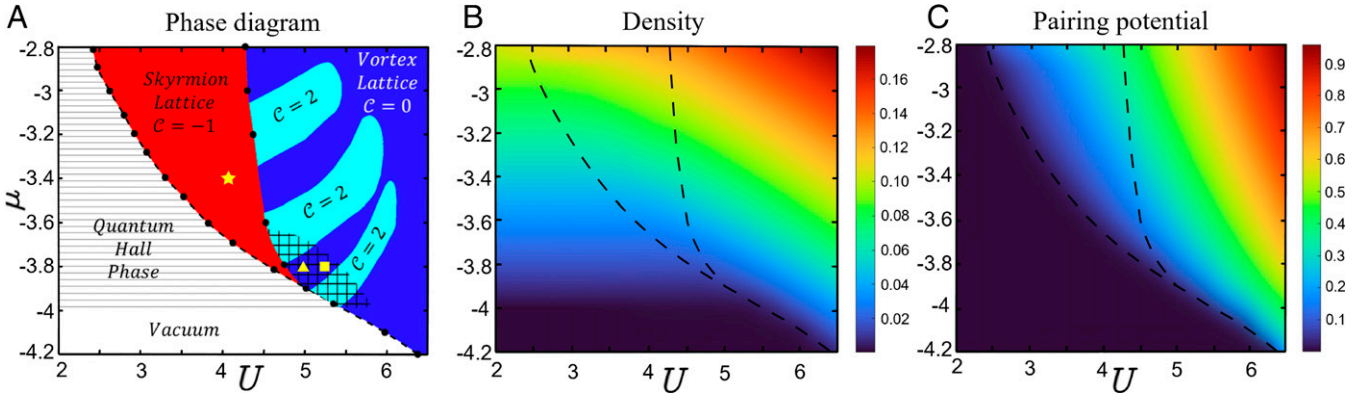

Fig. 2. (*A*) The mean-field phase diagram as a function of the magnitude of the nearest-neighbor attractive interaction U and the chemical potential μ, in units where the hopping amplitude is set to unity. Horizontal black lines in the quantum Hall phase indicate the energies of the Landau levels. The phase with skyrmion lattice region is marked in red. (The phase boundary separating the QHE and the skyrmion lattice phases is somewhat more complicated than that depicted. The boundary is constructed by taking the chemical potentials μ half-way between Landau levels; for μ closer to a LL energy, the skyrmion phase appears at smaller U. Also, skyrmion lattice phases with very high Chern numbers occur very close to the phase boundary, which have not been depicted to avoid clutter.) The regions with vortex lattice are indicated in blue and cyan, and the gridded region has competing vortex lattice/dimer vortex lattice phases. The yellow star, square, and triangle correspond to the skyrmion, vortex lattice, and dimer vortex lattice phases shown in Fig. 3, respectively. (*B*) The average particle number per site (density in units of a^{-2} where a is the lattice constant) as a function of μ and U. (*C*) Spatially averaged magnitude of the pairing potential as a function of μ and U. Note that the discontinuous changes in the spatially averaged pairing potential and the average density at the (first-order) phase transition are too small to be visible in the plots; for example, for $\mu = -3.6$, at the vortex lattice–skyrmion lattice phase boundary, the former is 0.006 (reflecting a 4% change in the magnitude) and the latter is 0.0002 (0.5%).

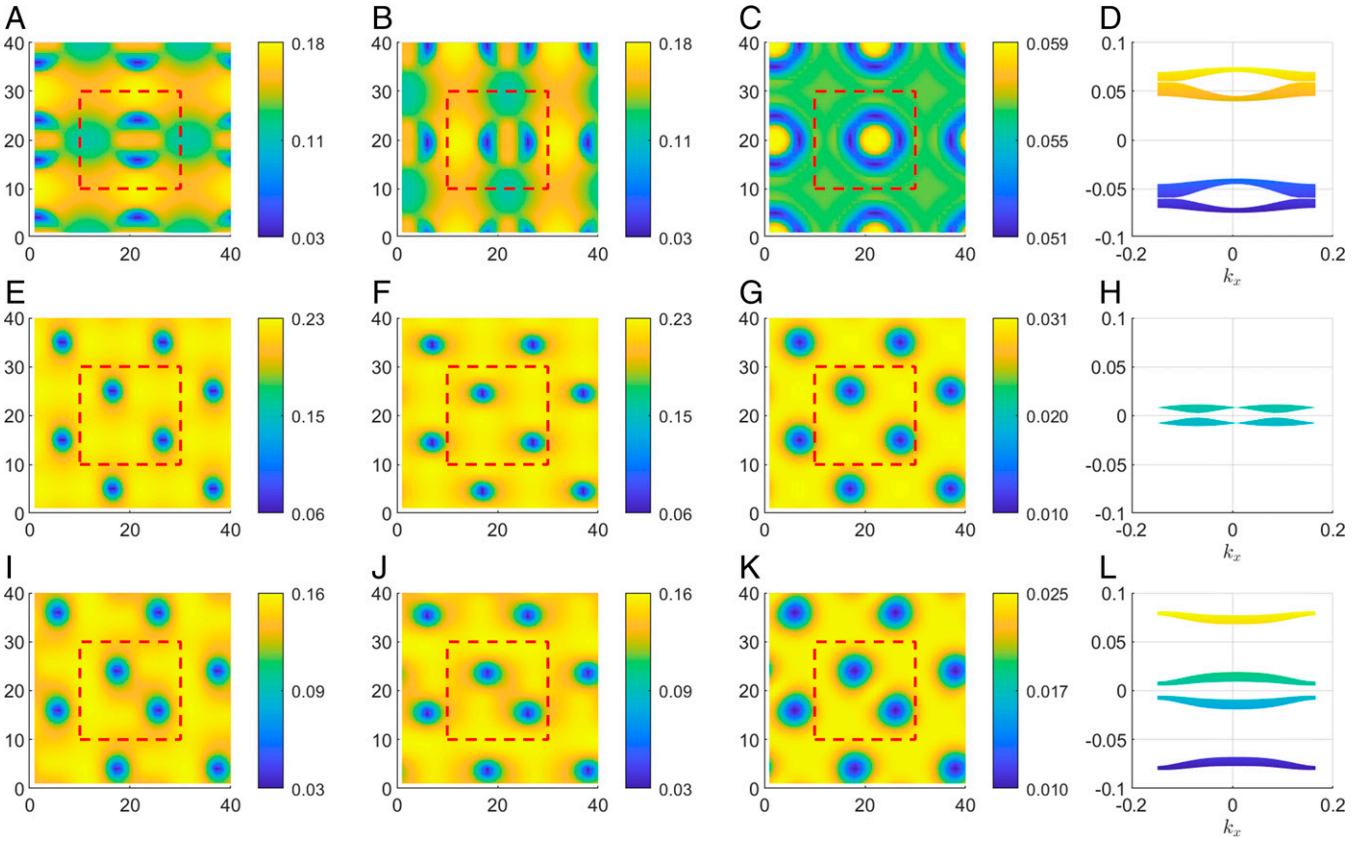

Fig. 3. (*A* and *B*) The magnitude of the components of the pairing potential $|\Delta_{j,x}|$ and $|\Delta_{j,y}|$. (*C*) The particle density. (*D*) The low-energy quasiparticle bands for the skyrmion lattice solution with $U = 4.05$ and $\mu = -3.4$. *E*–*H* show the same but for the vortex lattice solution with $U = 5.25$ and $\mu = -3.8$. *I*–*L* show the same but for the dimer lattice solution with $U = 5$ and $\mu = -3.8$. The red dashed lines denote the boundary of the MUC.

MUC is associated with h/e flux). The skyrmion has a ring structure in the density, as seen in Fig. 3*C*, which may provide a signature of skyrmions in scanning tunneling microscopy (STM) measurements. The fermionic spectrum in the skyrmion phase, shown in Fig. 3*D*, is gapped, indicating the absence of zero-energy Majorana-bound states in the bulk. The SC Chern number, computed using Eq. **16**, is $\mathcal{C} = -1$, signifying that it is in the phase of p-wave superconductors with non-Abelian excitations and has exactly one chiral Majorana edge mode.

It is useful to contrast the skyrmion phase with the more familiar vortex phase, which is discussed below. Unlike in the skyrmion phase, the vortices in each component occur at the same location in the vortex phase. Also, in the vortex phase the "total gap" $\sqrt{|\Delta_{j,x}|^2 + |\Delta_{j,y}|^2}$ almost vanishes at the locations of the vortices; for the skyrmion lattice, in contrast, the total gap is everywhere finite. Finally, the vortex phase has a low-energy Majorana band, which is absent in the skyrmion phase.

To classify the self-consistent solutions of the order parameter $\Delta_{j,\delta}$, it is convenient to define a topological invariant called the (real space) skyrmion number

$$\mathcal{Q} = \frac{1}{4\pi}\int \mathrm{d}^2\boldsymbol{r}\ \hat{\boldsymbol{n}}\cdot\left(\partial_x\hat{\boldsymbol{n}}\times\partial_y\hat{\boldsymbol{n}}\right), \qquad [21]$$

where the pseudospin vector $\hat{\boldsymbol{n}}$ is defined in terms of the superconducting order parameter in the continuum $\hat{n}_\alpha = \frac{\boldsymbol{\Delta}^\dagger\sigma_\alpha\boldsymbol{\Delta}}{\boldsymbol{\Delta}^\dagger\boldsymbol{\Delta}}$, where $\boldsymbol{\Delta} = (\Delta_x(\boldsymbol{r}), \Delta_y(\boldsymbol{r}))^T$ and σ is a Pauli matrix ($\alpha = x, y, z$). We expect $\mathcal{Q} = 0$ for vortex solutions and $\mathcal{Q} = 2$ for skyrmions (48). On the lattice, a problem arises with this definition of $\mathcal{Q}$. The order parameter transforms nonlocally under a gauge transformation $\hat{c}_j \to e^{i\phi_j}\hat{c}_j$, i.e., $\Delta_{j,\delta} \to e^{i(\phi_{j+\delta}+\phi_j)}\Delta_{j,\delta}$, and so the vector $\hat{\boldsymbol{n}}(\boldsymbol{r}_j)$ transforms as $\hat{\boldsymbol{n}}(\boldsymbol{r}_j) \to R_{xy}(\delta\theta)\hat{\boldsymbol{n}}(\boldsymbol{r}_j)$, where $R_{xy}(\delta\theta)$ is a rotation matrix in the xy plane by an angle $\delta\theta = \phi_{j+\hat{y}} - \phi_{j+\hat{x}}$. Consequently, the skyrmion number $\mathcal{Q}$ defined in this way is not invariant under gauge transformations on the lattice (the skyrmion number in the continuum, in contrast, is gauge invariant since there the continuum order parameter transforms locally under gauge transformations).

To construct a gauge-invariant skyrmion number on the lattice, we define the gauge-invariant phase difference between the components of the order parameter in the following way: We first define the phase of the two order parameters $\theta_{j,\delta}$,

$$\Delta_{j,\delta} = |\Delta_{j,\delta}|e^{i\theta_{j,\delta}}, \qquad [22]$$

where $\delta = x, y$. Instead of the bare phase, we consider the phase $\tilde{\theta}_{j,\delta} = \theta_{j,\delta} - A_{j+\delta,j}$, which by itself is not gauge invariant, but the combination $\tilde{\theta}_{j,y} - \tilde{\theta}_{j,x}$ is gauge invariant:

$$\begin{aligned}\tilde{\theta}_{j,y} - \tilde{\theta}_{j,x} \to &\theta_{j,y} + \phi_j + \phi_{j+\hat{y}} - \left(A_{j+\hat{y},j} + \phi_{j+\hat{y}} - \phi_j\right)\\ &-\theta_{j,x} - \phi_j - \phi_{j+\hat{x}} + \left(A_{j+\hat{x},j} + \phi_{j+\hat{x}} - \phi_j\right)\\ =&\left(\theta_{j,y} - A_{j+\hat{y},j}\right) - \left(\theta_{j,x} - A_{j+\hat{x},j}\right)\\ =&\tilde{\theta}_{j,y} - \tilde{\theta}_{j,x}. \end{aligned} \qquad [23]$$

This motivates us to define a pseudospin vector on the lattice using $\tilde{\theta}_{j,\delta}$:

$$\hat{n}_{j,\alpha} = \frac{\boldsymbol{\Delta}_j^\dagger\sigma_\alpha\boldsymbol{\Delta}_j}{\boldsymbol{\Delta}_j^\dagger\boldsymbol{\Delta}_j}, \quad \text{where} \quad \boldsymbol{\Delta}_j = \begin{pmatrix}|\Delta_{j,x}|e^{i\tilde{\theta}_{j,x}}\\ |\Delta_{j,y}|e^{i\tilde{\theta}_{j,y}}\end{pmatrix}. \qquad [24]$$

The pseudospin $\hat{n}_{j,\alpha}$ is gauge invariant on the lattice and the skyrmion number, computed using a lattice-discretized version of Eq. **21**, is $\mathcal{Q} = 2$ for a skyrmion and $\mathcal{Q} = 0$ for two vortices (both evenly spaced and dimer vortices discussed below) when rounded to the nearest integer. This is consistent with the values found in continuum systems (48, 49, 51). Furthermore, it can be shown that the lattice pseudospin vector is identical to the continuum pseudospin vector, defined above, in the continuum limit. Therefore, we conclude that the deviation of the lattice skyrmion number from an integer is a result of lattice discretization; using a finer lattice (i.e., more sites per MUC) will yield skyrmion numbers closer to their continuum limit values.

It is also instructive to look at the spatial variation of the (gauge-invariant) phase difference $\tilde{\theta}_{j,y} - \tilde{\theta}_{j,x}$ in the skyrmion phase. Fig. 4 shows the cosine and sine of the angle difference for the skyrmion phase. The cosine shows alternating sign between the half-quantum vortices, a signature of skyrmions in p-wave superconductors (51). The sine plot displays another defining feature of skyrmions in this context—closed domains of inverted chirality. In the present case, the pairing symmetry is $p_x + ip_y$ (the phase difference is $\pi/2$) inside the skyrmion, and outside it is $p_x - ip_y$ (the phase difference is $-\pi/2$). The half-quantum vortices reside on this domain wall. We note that the phase difference plots for the vortex and dimer vortex phase are comparatively featureless—the phase difference is pinned to $\pi/2$, implying that the entire system has $p_x + ip_y$ pairing symmetry.

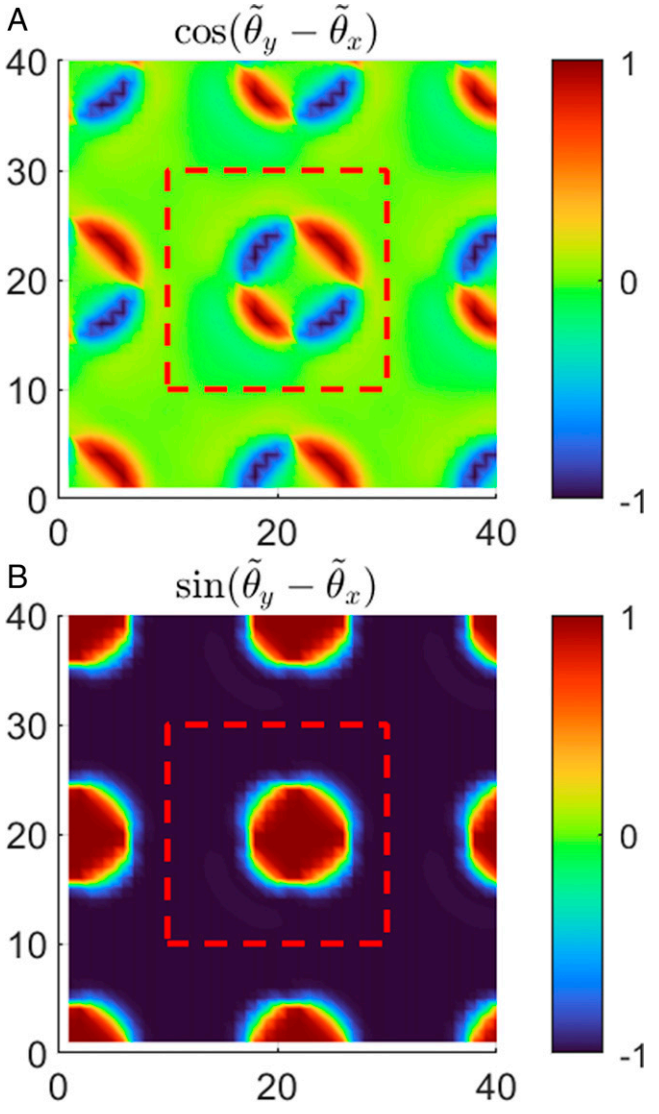

Fig. 4. (*A*) The cosine of the gauge-invariant phase difference between the *x* and *y* components of the order parameter for the skyrmion phase. Along the boundary of the skyrmion, the pairing symmetry oscillates between $p_x + p_y$ and $p_x - p_y$. (*B*) The sine of the gauge-invariant phase difference between the *x* and *y* components of the order parameter for the skyrmion phase. Inside the skyrmion, the pairing symmetry is $p_x + ip_y$, and outside, the pairing symmetry is $p_x - ip_y$.

C. Vortex Lattice and Dimerized-Vortex Lattice. The region where the ground state forms a vortex lattice is indicated by blue and cyan in Fig. 2, with SC Chern numbers equal to $\mathcal{C} = 0$ and $\mathcal{C} = 2$, respectively. The vortex lattice solution is energetically favored in the superconducting region when the chemical potential is low or the interaction strength is high. Note that for low chemical potentials the transition is directly from the QH phase into the vortex lattice phase.

The magnitudes of the two components of the order parameter, $|\Delta_{j,x}|$ and $|\Delta_{j,y}|$; the particle density; and the low-energy BdG quasiparticle band structure for the vortex lattice phase are shown in Fig. 3 *E*–*H*. The vortices in each component occur at the same location and form a square lattice. Note that the total gap $\sqrt{|\Delta_{j,x}|^2 + |\Delta_{j,y}|^2}$ almost vanishes at the locations of the vortices. The vortex lattice phase has a low-energy band structure (shown in Fig. 3*H*) that is consistent with the findings of previous studies of Majorana bands (40, 57–68), where the dynamics were described by Majoranas hopping between vortices with nearest-neighbor and next–nearest-neighbor hopping. The spectrum has a small gap and we find that the Chern number is $\mathcal{C} = 0, 2$ in the vortex phase, which is also consistent with previous studies (37, 67). This supports the claim that the non-Abelian phase is not possible for a lattice of vortices with one vortex per vortex unit cell (36, 37, 67).

Additionally, we find that vortices show a tendency to dimerize (i.e., form a lattice with two vortices per vortex unit cell). This phase is energetically competitive in the black gridded region of the phase diagram; for some parameters it is the clear ground state whereas in other cases it is only slightly higher in energy than the vortex lattice solution. It is also found as a higher-energy self-consistent solution in much of the phase diagram. The magnitudes of the two components of the order parameter, $|\Delta_{j,x}|$ and $|\Delta_{j,y}|$; the particle density; and the low-energy BdG quasiparticle band structure for the dimer vortex lattice phase are shown in Fig. 3 *I*–*L*. As can be seen, the vortices are not equally spaced. This breaks the vortex magnetic translation symmetry (35, 36) and allows for odd SC Chern number and hence the non-Abelian phase. We find that the SC Chern number $\mathcal{C} = 1$ is the same as that of the background $p_x + ip_y$ superconductor. It is encouraging to find that the system breaks the vortex translation symmetry all on its own; translation symmetry-breaking perturbations may thus not be required to realize the non-Abelian phase of vortex lattices in p-wave superconductors (36, 61, 63).

The current textures for the skyrmion, vortex, and dimer vortex lattice phases are shown in Fig. 5. The current is determined by evaluating the expectation value of the current operator

$$\hat{J}_{j,\delta} = i\left(e^{iA_{j+\delta,j}}\hat{c}^{\dagger}_{j+\delta}\hat{c}_j - e^{iA_{j,j+\delta}}\hat{c}^{\dagger}_j\hat{c}_{j+\delta}\right) \qquad [25]$$

in the ground state. This expression can be derived by considering variation of the Hamiltonian with respect to the hopping phases or by using the continuity equation (69). The current texture for a skyrmion (shown in Fig. 5*A*) shows inner and outer currents

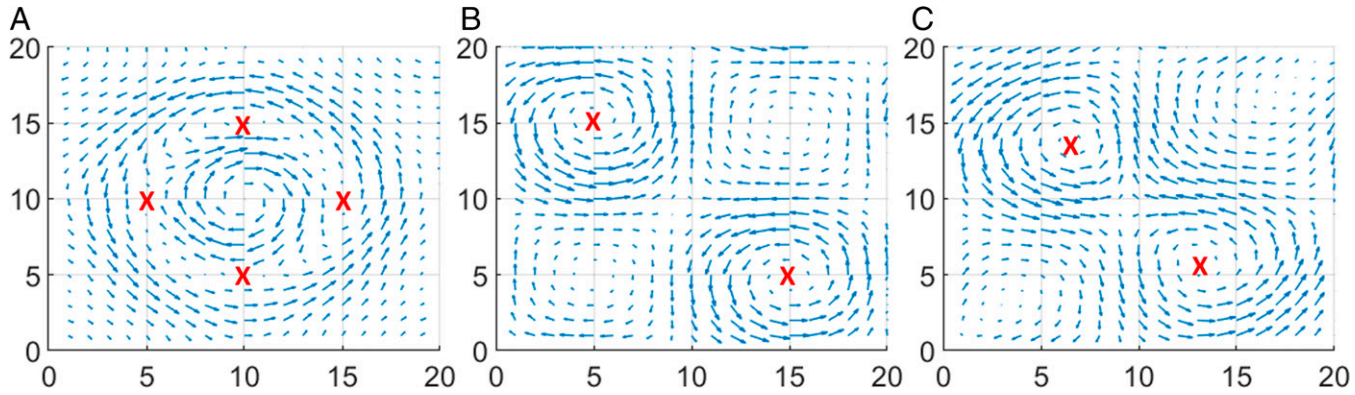

Fig. 5. (*A*–*C*) The current texture for a skyrmion (*A*), a pair of vortices in a vortex lattice (*B*), and pair of vortex dimers (*C*). Half-vortices in *A* and vortices in *B* and *C* are marked by **X**.

flowing in opposite directions. This structure can be understood as coming from the combined supercurrent of the bound half-quantum vortices. The vortex lattice phase (Fig. 5*B*) shows relatively separated current circulation for each vortex whereas for the vortex dimers (Fig. 5*C*) the current percolates between the vortices in the dimer.

The spatially averaged pairing potential and the average density are also shown in Fig. 2 *B* and *C*. The discontinuous jumps in these quantities at the (first-order) phase boundary separating the vortex lattice–skyrmion lattice phases are small because they arise primarily from the regions in the immediate vicinity of the vortices and the skyrmions. For example, for $\mu = -3.6$, the change in the spatially averaged pairing potential is 0.006 (reflecting a 4% change in the magnitude) and that in the average density is 0.0002 (0.5% change in the magnitude). These jumps are not visible in Fig. 2 *B* and *C*. The QHE to skyrmion lattice transition is also first order, as expected from the large change in the Chern number. Here we find that the average pairing potential jumps from zero to a number approximately equal to twice the energy separation between μ and the nearest LL.

Discussion

Despite the attention that vortices have received in the context of topological p-wave superconductivity in QH systems, the question of whether or not the vortex lattices are the stable self-consistent ground-state solutions has been relatively unexplored. Nevertheless, recent studies have pointed out that systems with a regular lattice of Abrikosov vortices carrying flux $h/2e$ have an even SC Chern number $\mathcal{C}$, due to the vortex magnetic translation symmetry that enforces an even number of Dirac crossings, and hence these systems have the same classification as the QH phase with fermionic (as opposed to Majorana) chiral edge modes (36, 37, 67). These results are indeed consistent with ours, for the portion of the phase diagram at relatively strong pairing strength, but we find cases where the system seems to circumvent this problem by forming skyrmions or vortex dimers, thereby allowing for odd SC Chern number and hence chiral Majorana edge modes.

Some insight into the origin of the vortex dimer phase can be gained by analogy to Peierls-type physics: A Peierls distortion opens a larger gap, pushing the states near zero energy to lower energies, as shown in Fig. 3 *D*, *H*, and *L*, thereby reducing the energy of the Majorana band. However, whether such distortion actually occurs depends on other bands as well as the last term in Eq. **12**. Similarly, the formation of skyrmions also opens a large gap at the Fermi energy that can stabilize it in some parameter regimes.

It should be noted that our choice of a square MUC containing one quantum of flux h/e, which is limited by the need of computational resources, forces the skyrmions, Abrikosov vortices, and vortex dimers to all form a square lattice. Choosing a larger number of magnetic flux quanta per MUC would constrain the lattice to a lesser degree and could allow for a triangular lattice of vortices. Although the lattice type may change, we expect the phase diagram to qualitatively remain the same, especially when the skyrmions, vortices, and vortex dimers are far separated.

A comment on the center-of-mass (COM) magnetic momentum of the Cooper pairs is also in order. Our assumption that the mean-field pairing potential $\Delta_{j,\delta}$ has the same periodicity as the MUC of the noninteracting system (described by the Hamiltonian $\mathcal{H}_0$) allows only for pairing between fermions of opposite magnetic momenta $\boldsymbol{k}$ and $-\boldsymbol{k}$, resulting in Cooper pairs with zero COM magnetic momentum. (A nonzero COM momentum would manifest through a phase twist across an MUC.) In studies of the SC Hofstadter model in large magnetic fields, pairing instabilities can also occur at finite COM momentum, due to degeneracies arising from the magnetic translation symmetry, leading to Fulde–Ferrell–Larkin–Ovchinnikov (FFLO) superconductivity (70–73). We neglect in our work FFLO pairing because our interest has primarily to do with skyrmion/Majorana physics in the continuum limit and also because FFLO pairing has not yet been decisively observed in condensed-matter systems.

We end with a remark on the experimental relevance of our results. We expect our model with nearest-neighbor attractive interaction to be relevant to p-wave superconductors under external magnetic fields. In addition, our study will provide a guidance to understand physics in s-wave superconductors with strong spin–orbit coupling under an external magnetic field or in heterostructures consisting of a 2D SC coupled to a 2D QH system.

Data Availability. The program used to generate the data in this article may be accessed on Zenodo at https://doi.org/10.5281/zenodo.6656573 (74). All study data are included in this article and/or *SI Appendix*.

ACKNOWLEDGMENTS. We are grateful to Egor Babaev and Mohit Randeria for enlightening discussions. J.S. thanks Prachi Singh for help with figures. J.S. and J.K.J. were supported in part by the US Department of Energy, Office of Basic Energy Sciences, under Grant DE-SC-0005042. We acknowledge Advanced CyberInfrastructure computational resources provided by The Institute for CyberScience at The Pennsylvania State University. J.S. and C.-X.L. acknowledge the partial support from New Initiative Research Grant KA2018-98553 of the Pittsburgh Foundation. C.-X.L. also acknowledges the partial support from the office of Naval Research (Grant N00014-18-1-2793) and NSF through Princeton University's Materials Research Science and Engineering Center (DMR-2011750).

1. K. Klitzing, G. Dorda, M. Pepper, New method for high-accuracy determination of the fine-structure constant based on quantized Hall resistance. *Phys. Rev. Lett.* **45**, 494 (1980).
2. D. J. Thouless, M. Kohmoto, M. P. Nightingale, M. den Nijs, Quantized Hall conductance in a two-dimensional periodic potential. *Phys. Rev. Lett.* **49**, 405–408 (1982).
3. J. Leinaas, J. Myrheim, On the theory of identical particles. *Nuovo Cim. B Ser. 11* **37**, 1–23.
4. F. Wilczek, Magnetic flux, angular momentum, and statistics. *Phys. Rev. Lett.* **48**, 1144 (1982).
5. Y. S. Wu, General theory for quantum statistics in two dimensions. *Phys. Rev. Lett.* **52**, 2103 (1984).
6. E. Majorana, Theory of the symmetry of electrons and positrons. *Nuovo Cim.* **14**, 50 (1937).
7. N. Read, D. Green, Paired states of fermions in two dimensions with breaking of parity and time-reversal symmetries and the fractional quantum Hall effect. *Phys. Rev. B* **61**, 10267 (2000).
8. D. A. Ivanov, Non-Abelian statistics of half-quantum vortices in p-wave superconductors. *Phys. Rev. Lett.* **86**, 268–271 (2001).
9. A. Y. Kitaev, Unpaired Majorana fermions in quantum wires. *Phys. Uspekhi* **44** (10S), 131–136 (2001).
10. M. Stone, S. B. Chung, Fusion rules and vortices in $p_x + ip_y$ superconductors. *Phys. Rev. B* **73**, 014505 (2006).
11. L. Fu, C. L. Kane, Superconducting proximity effect and Majorana fermions at the surface of a topological insulator. *Phys. Rev. Lett.* **100**, 096407 (2008).
12. F. Wilczek, Majorana returns. *Nat. Phys.* **5**, 614–618 (2009).
13. X. L. Qi, T. L. Hughes, S. C. Zhang, Chiral topological superconductor from the quantum Hall state. *Phys. Rev. B* **82**, 184516 (2010).
14. J. D. Sau, R. M. Lutchyn, S. Tewari, S. Das Sarma, Generic new platform for topological quantum computation using semiconductor heterostructures. *Phys. Rev. Lett.* **104**, 040502 (2010).
15. M. Leijnse, K. Flensberg, Introduction to topological superconductivity and Majorana fermions. *Semicond. Sci. Technol.* **27**, 124003 (2012).
16. C. Beenakker, Search for Majorana fermions in superconductors. *Annu. Rev. Condens. Matter Phys.* **4**, 113–136 (2013).
17. J. Alicea, A. Stern, Designer non-Abelian anyon platforms: From Majorana to Fibonacci. *Phys. Scr. T* **164**, 014006 (2015).
18. S. R. Elliott, M. Franz, Colloquium: Majorana fermions in nuclear, particle, and solid-state physics. *Rev. Mod. Phys.* **87**, 137–163 (2015).
19. F. Amet *et al.*, Supercurrent in the quantum Hall regime. *Science* **352**, 966–969 (2016).
20. G. H. Lee *et al.*, Inducing superconducting correlation in quantum Hall edge states. *Nat. Phys.* **13**, 693 (2017).
21. M. R. Sahu *et al.*, Inter-Landau-level Andreev reflection at the Dirac point in a graphene quantum Hall state coupled to a NbSe 2 superconductor. *Phys. Rev. Lett.* **121**, 086809 (2018).
22. L. Zhao *et al.*, Interference of chiral Andreev edge states. *Nat. Phys.* **16**, 862–867 (2020).
23. D. C. Tsui, H. L. Stormer, A. C. Gossard, Two-dimensional magnetotransport in the extreme quantum limit. *Phys. Rev. Lett.* **48**, 1559–1562 (1982).
24. A. Kitaev, Fault-tolerant quantum computation by anyons. *Ann. Phys.* **303**, 2–30 (2003).
25. M. Freedman, A. Kitaev, M. Larsen, Z. Wang, Topological quantum computation. *Bull. Am. Math. Soc.* **40**, 31–38 (2003).
26. S. D. Sarma, C. Nayak, S. Tewari, Proposal to stabilize and detect half-quantum vortices in strontium ruthenate thin films: Non-Abelian braiding statistics of vortices in a $p_x + ip_y$ superconductor. *Phys. Rev. B* **73**, 220502 (2006).
27. S. Tewari, S. Das Sarma, C. Nayak, C. Zhang, P. Zoller, Quantum computation using vortices and Majorana zero modes of a $p_x + ip_y$ superfluid of fermionic cold atoms. *Phys. Rev. Lett.* **98**, 010506 (2007).
28. C. Nayak, S. H. Simon, A. Stern, M. Freedman, S. Das Sarma, Non-Abelian anyons and topological quantum computation. *Rev. Mod. Phys.* **80**, 1083–1159 (2008).
29. J. Alicea, New directions in the pursuit of Majorana fermions in solid state systems. *Rep. Prog. Phys.* **75**, 076501 (2012).
30. J. K. Pachos, *Introduction to Topological Quantum Computation* (Cambridge University Press, 2012).
31. T. D. Stanescu, S. Tewari, Majorana fermions in semiconductor nanowires: Fundamentals, modeling, and experiment. *J. Phys. Condens. Matter* **25**, 233201 (2013).
32. R. S. Mong *et al.*, Universal topological quantum computation from a superconductor-Abelian quantum Hall heterostructure. *Phys. Rev. X* **4**, 011036 (2014).
33. J. K. Jain, It's anyon's game: The race to quantum computation. *Curr. Sci.* **119**, 430–432 (2020).
34. B. Zocher, B. Rosenow, Topological superconductivity in quantum Hall–superconductor hybrid systems. *Phys. Rev. B* **93**, 214504 (2016).
35. G. S. Jeon, J. Jain, C. X. Liu, Topological superconductivity in Landau levels. *Phys. Rev. B* **99**, 094509 (2019).
36. R. V. Mishmash, A. Yazdani, M. P. Zaletel, Majorana lattices from the quantized Hall limit of a proximitized spin-orbit coupled electron gas. *Phys. Rev. B* **99**, 115427 (2019).
37. G. Chaudhary, A. H. MacDonald, Vortex-lattice structure and topological superconductivity in the quantum Hall regime. *Phys. Rev. B* **101**, 024516 (2020).
38. G. Chaudhary, A. MacDonald, M. Norman, Quantum Hall superconductivity from moiré Landau levels. *Phys. Rev. Res.* **3**, 033260 (2021).
39. O. Vafek, A. Melikyan, M. Franz, Z. Tešanović, Quasiparticles and vortices in unconventional superconductors. *Phys. Rev. B* **63**, 134509 (2001).
40. T. Liu, M. Franz, Electronic structure of topological superconductors in the presence of a vortex lattice. *Phys. Rev. B* **92**, 134519 (2015).
41. V. Pathak, S. Plugge, M. Franz, Majorana bound states in vortex lattices on iron-based superconductors. *Ann. Phys.* **435**, 168431 (2021).
42. M. Franz, Z. Tešanović, Quasiparticles in the vortex lattice of unconventional superconductors: Bloch waves or Landau levels? *Phys. Rev. Lett.* **84**, 554–557 (2000).
43. B. Rosenstein, D. Li, Ginzburg-Landau theory of type II superconductors in magnetic field. *Rev. Mod. Phys.* **82**, 109 (2010).
44. M. Takigawa, M. Ichioka, K. Machida, M. Sigrist, Vortex structure in chiral p-wave superconductors. *Phys. Rev. B* **65**, 014508 (2001).
45. E. Babaev, Vortices with fractional flux in two-gap superconductors and in extended Faddeev model. *Phys. Rev. Lett.* **89**, 067001 (2002).
46. Q. Li, J. Toner, D. Belitz, Skyrmion versus vortex flux lattices in p-wave superconductors. *Phys. Rev. B* **79**, 014517 (2009).
47. E. Babaev, J. Carlström, J. Garaud, M. Silaev, J. Speight, Type-1.5 superconductivity in multiband systems: Magnetic response, broken symmetries and microscopic theory–a brief overview. *Physica C* **479**, 2–14 (2012).
48. J. Garaud, E. Babaev, Skyrmionic state and stable half-quantum vortices in chiral p-wave superconductors. *Phys. Rev. B* **86**, 060514 (2012).
49. J. Garaud, E. Babaev, Properties of skyrmions and multi-quanta vortices in chiral p-wave superconductors. *Sci. Rep.* **5**, 17540 (2015).
50. E. Babaev, J. Carlström, M. Silaev, J. Speight, *Superconductors at the Nanoscale* (de Gruyter, 2017).
51. V. F Becerra, E. Sardella, F. M. Peeters, M. V. Milošević, Vortical versus skyrmionic states in mesoscopic p-wave superconductors. *Phys. Rev. B* **93**, 014518 (2016). https://doi.org/10.1103/PhysRevB.93.014518.
52. L. F. Zhang, V. F. Becerra, L. Covaci, M. Milošević, Electronic properties of emergent topological defects in chiral p-wave superconductivity. *Phys. Rev. B* **94**, 024520 (2016).
53. D. R. Hofstadter, Energy levels and wave functions of Bloch electrons in rational and irrational magnetic fields. *Phys. Rev. B* **14**, 2239 (1976).
54. A. Altland, M. R. Zirnbauer, Nonstandard symmetry classes in mesoscopic normal-superconducting hybrid structures. *Phys. Rev. B* **55**, 1142 (1997).
55. T. Fukui, Y. Hatsugai, H. Suzuki, Chern numbers in discretized brillouin zone: Efficient method of computing (spin) hall conductances. *J. Phys. Soc. Jpn.* **74**, 1674–1677 (2005).
56. M. Aidelsburger, *Artificial Gauge Fields With Ultracold Atoms in Optical Lattices* (Springer, 2015).
57. E. Grosfeld, A. Stern, Electronic transport in an array of quasiparticles in the $\nu = 5/2$ non-abelian quantum hall state. *Phys. Rev. B* **73**, 201303 (2006).
58. M. Cheng, R. M. Lutchyn, V. Galitski, S. Das Sarma, Splitting of Majorana-fermion modes due to intervortex tunneling in a $p_{(x)} + ip_{(y)}$ superconductor. *Phys. Rev. Lett.* **103**, 107001 (2009).
59. M. Cheng, R. M. Lutchyn, V. Galitski, S. Das Sarma, Tunneling of anyonic majorana excitations in topological superconductors. *Phys. Rev. B Condens. Matter Mater. Phys.* **82**, 094504 (2010).
60. A. W. Ludwig, D. Poilblanc, S. Trebst, M. Troyer, Two-dimensional quantum liquids from interacting non-abelian anyons. *New J. Phys.* **13**, 045014 (2011).
61. Y. E. Kraus, A. Stern, Majorana fermions on a disordered triangular lattice. *New J. Phys.* **13**, 105006 (2011).
62. V. Lahtinen, A. W. Ludwig, J. K. Pachos, S. Trebst, Topological liquid nucleation induced by vortex-vortex interactions in kitaev's honeycomb model. *Phys. Rev. B* **86**, 075115 (2012).
63. C. R. Laumann, A. W. Ludwig, D. A. Huse, S. Trebst, Disorder-induced majorana metal in interacting non-abelian anyon systems. *Phys. Rev. B* **85**, 161301 (2012).
64. J. Zhou, Y. J. Wu, R. W. Li, J. He, S. P. Kou, Hierarchical topological superconductor–a majorana vortex lattice model. *EPL* **102**, 47005 (2013). (Europhysics Letters).
65. R. R. Biswas, Majorana fermions in vortex lattices. *Phys. Rev. Lett.* **111**, 136401 (2013).
66. M. Silaev, Majorana fermions on the abrikosov flux lattice in a $p_x + ip_y$ superconductor. *Phys. Rev. B* **88**, 064514 (2013).
67. J. M. Murray, O. Vafek, Majorana bands, Berry curvature, and thermal Hall conductivity in the vortex state of a chiral p-wave superconductor. *Phys. Rev. B* **92**, 134520 (2015).
68. D. Ariad, E. Grosfeld, B. Seradjeh, Effective theory of vortices in two-dimensional spinless chiral p-wave superfluids. *Phys. Rev. B* **92**, 035136 (2015).
69. H. Watanabe, A proof of the bloch theorem for lattice models. *J. Stat. Phys.* **177**, 717–726 (2019).
70. H. Zhai, R. O. Umucalilar, M. O. Oktel, Pairing and vortex lattices for interacting fermions in optical lattices with a large magnetic field. *Phys. Rev. Lett.* **104**, 145301 (2010).
71. S. Powell, R. Barnett, R. Sensarma, S. Das Sarma, Interacting Hofstadter spectrum of atoms in an artificial gauge field. *Phys. Rev. Lett.* **104**, 255303 (2010).
72. R. Sohal, E. Fradkin, Intertwined order in fractional Chern insulators from finite-momentum pairing of composite fermions. *Phys. Rev. B* **101**, 245154 (2020).
73. D. Shaffer, J. Wang, L. H. Santos, Theory of hofstadter superconductors. *Phys. Rev. B* **104**, 184501 (2021).
74. J. Schirmer, Program for "Phase diagram of superconductivity in the integer quantum Hall regime." Zenodo. https://zenodo.org/record/6656573#.YrxkH3bMLIU. Deposited 20 June 2022.